Welding in the World
https://doi.org/10.1007/s40194-025-02139-7

RESEARCH PAPER

Fatigue behavior of thermal cut edges in normal- and high-strength steel: effect of defined post-processing treatment

Jan-Hendrik Grimm[1] · Markus Köhler[2] · Moritz Braun[1,3] · Franz von Bock und Polach[1] · Klaus Dilger[2] · Sören Ehlers[1,3]

Received: 12 December 2024 / Accepted: 25 July 2025

Abstract
Within ships or maritime structures, plate edges are an important detail for the strength and fatigue assessment. Large openings such as hatches on container vessels or windows on cruise ships lead to a stress concentration, which has to be considered for strength calculation. These openings within steel plates are generally manufactured by thermal cutting processes. The recommendations regarding fatigue design by the IIW and classification societies for the structural behavior of these details are limited to general design categories using the nominal stress approach. In addition, no strict differences in cutting technologies and edge treatments such as grinding are taken into account. The aim of this investigation is to present the potential of a defined edge treatment for thermal cut edges on the fatigue performance. Therefore, fatigue tests with constant amplitudes were carried out and the specimens are characterized by identifying important properties such as roughness and hardness. This paper describes the fatigue behavior of thermal cut edges made of structural steel plates with different thicknesses from 5 to 25 mm including steel grades from S235 up to S690. All specimens were manufactured in an acceptable and comparable quality range according to ISO 9013, quality level 2, and have been treated with a defined chamfer to compare the influences of cutting processes and yield levels. Previous studies already indicated a beneficial effect regarding fatigue strength of thermal cut edges using higher strength steels, but the results were not clearly in line to describe the behavior sufficiently. This study demonstrates and confirms that material effects and a targeted post-treatment have a beneficial impact on the fatigue behavior of thermal cut edges. A continuous increase in the achieved stress ranges was observed with increasing steel strength. Based on the observations made, an approach for predicting the achievable fatigue strength is presented, taking surface roughness and material strength into account.

Keywords Thermal cut edges · Post-processing treatment · Fatigue tests · Yield effects · Surface quality

1 Introduction and State of the Art

For ships and maritime structures, strength assessments of the overall structure are carried out during the design phase as well as during operation. The applicable requirements are defined by the regulations of classification societies, e.g., DNV [1, 2], and more general structural steel design recommendations like the International Institute of Welding (IIW) [3] or Eurocode 3 [4]. Strength verification generally involves evaluating a structure for specified static and dynamic loads. Particularly, ships and all offshore structures experience continuous dynamic loading during operation, primarily due to wave-induced forces, e.g., presented by Fricke et al. [5], Li et al. [6], and Storhaug et al. [7]. For assessing the fatigue behavior of maritime constructions, the verification of operational strength is of

Recommended for publication by Commission XIII - Fatigue of Welded Components and Structures

✉ Jan-Hendrik Grimm
jan.grimm@tuhh.de

[1] Institute for Ship Structural Design and Analysis, Hamburg University of Technology, Hamburg, Germany

[2] Institute of Joining and Welding, Technische Universität Braunschweig, Braunschweig, Germany

[3] German Aerospace Center (DLR), Institute of Maritime Energy Systems, Geesthacht, Germany

Published online: 08 September 2025

particular importance. This verification ensures that the structure can withstand dynamic loading over a predetermined design lifetime, thereby ensuring safe operation for the ship or offshore structure.

To determine the global structural behavior, computational models are typically employed, which represent the entire structure using finite element analysis (FEA) and provide information on the stresses occurring in the ship hull or an offshore construction. For local assessments, smaller sub-models are utilized to represent specific construction details and more precisely evaluate local effects. The focus in operational strength verification of large steel structures is often on the assessment of welds, which generally constitute the most critical details due to their high stress concentration. However, the evaluation of cut edges also plays a significant role, especially in the case of large cutouts or highly loaded corner brackets. Other examples of free cut edges include hatch corners, door and window openings, and penetrations in web frames for profiles. In ships, many of these cutouts are found in areas subject to high stresses, necessitating reliable utilization to prevent crack formation and structural failure. The general layout of these corners and a typical local FEA calculation is illustrated in Fig. 1. The fatigue performance of these details is generally evaluated by testing specimens, and the resulting directives are incorporated into relevant guidelines and standards, e.g., IIW [3] or DNV [1].

1.1 Research gaps and aim

In addition to the shipbuilding regulations, the general recommendations focused on steel construction by the International Institute of Welding (IIW) [3] and Eurocode 3 [4] are also relevant for fatigue strength verification. A common part of all these regulations is the ability to assess relevant details using the nominal stress approach. For this approach, nominal stresses from global calculation models or analytically determined stresses can be used for the fatigue lifetime assessment. The given design stress-life (S–N) curves for thermal cut edges are in a range from FAT 80 up to FAT 140. DNV-CG-0129 [1] includes an even higher curve (FAT 150) based on the requirement of a more detailed stress analysis using FEA. Within this guideline an additional curve FAT 235 is mentioned for steels with yield strengths above 500 MPa.

In the nominal stress concept, the evaluation is carried out based on numerous detail categories, also referred to as FAT classes, with design S–N curves characterized by a defined slope and a fatigue strength value at $2 \cdot 10^6$ load cycles. This concept is particularly relevant for the free plate edges found at cutouts and openings, and is a common practice in industrial applications. A compilation of the usual FAT classes according to IIW [3] in the S–N diagram is shown in Fig. 2. The design S–N curves for higher quality cut edges FAT 125 and FAT 140 shown by IIW exhibit a slope of m = 5

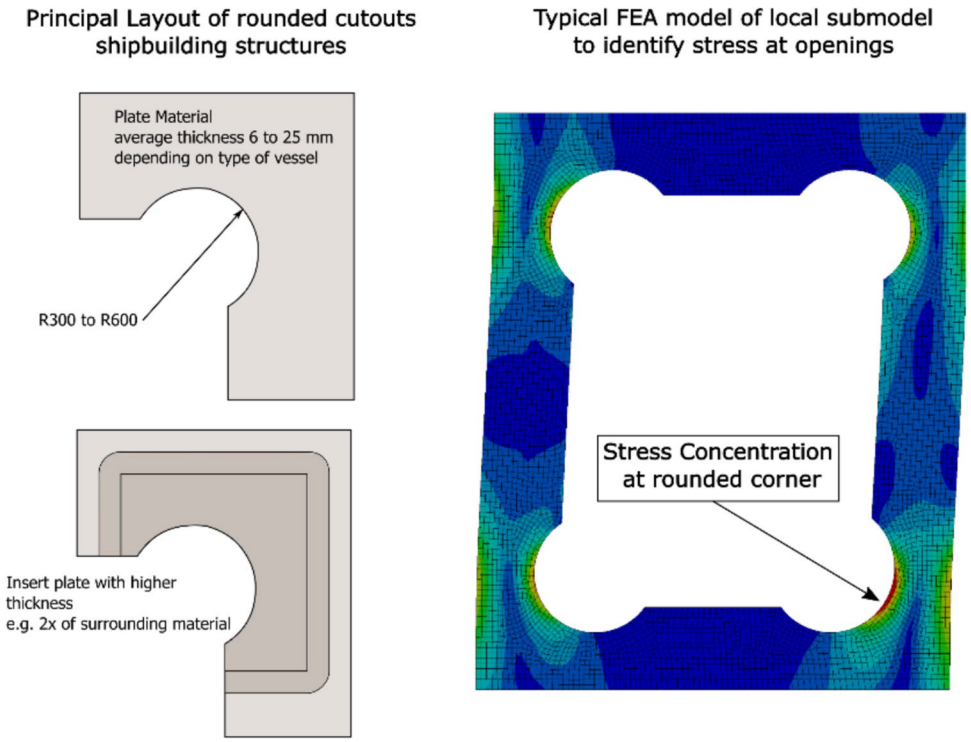

Fig. 1 Typical layout of rounded corners within maritime structures showing different radii and insert plate for reduction of local stresses (left); Example of principle local FE analysis of window opening in ships to identify occurring stresses (right)

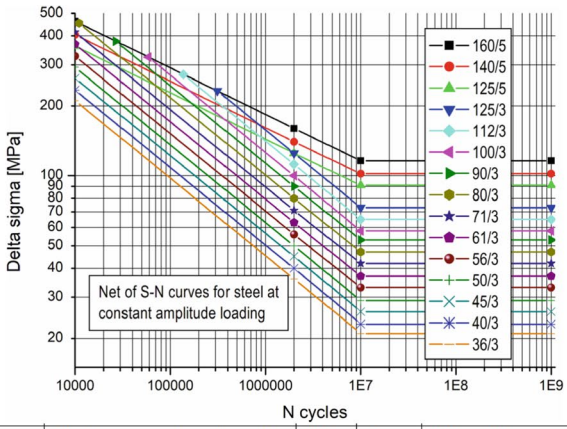

121	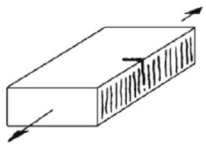	Machine gas cut or sheared material with subsequent dressing, no cracks by inspection, no visible imperfections m = 5	140	45	All visible signs of edge imperfections to be removed. The cut surfaces to be machined or ground, all burrs to be removed. No repair by welding refill Notch effects due to shape of edges shall be considered.
122	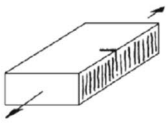	Machine thermally cut edges, corners removed, no cracks by inspection m = 5	125	40	Notch effects due to shape of edges shall be considered.

Fig. 2 Design S–N curves by IIW (top) and relevant categories FAT 125 and FAT 140 thermal cut edges in good manufacturing condition (bottom); both [3]

for the finite life range. Only the curve for base materials is provided even higher with a FAT 160 value and a slope of m = 5 in the recommendations. Further, no distinction is made regarding the cutting process or the yield strength of the material. Both mentioned design curves for free plate edges require a machine cutting process and no manufacturing by hand. For the highest classification of this detail with a FAT 140 value, there is an additional requirement that the cut edges must be ground and free from notches. There is no further description on the execution of the edge treatment. The relevant detail categories are listed in Fig. 2. Similar requirements, apart from a steeper slope exponent, can be found in Eurocode 3 [4], which is relevant for steel construction. The maximum design S–N curve there also reaches FAT 140 with a slope of m = 3.

Maritime regulations like those from DNV [1] use comparable approaches and distinctions in detail categories. However, in the current recommendations, a slightly steeper slope of the curves is indicated with increasing FAT values compared to IIW. The highest design S–N curves, FAT 140 and FAT 150, are both noted with a slope of m = 4. For the highest classification, FAT 150, an edge treatment of the geometry with a grinding process in the longitudinal direction, is required. Additionally, in this case, a local calculation of the local stresses for the detail to be designed is required. There is no distinction between the thermal cutting processes and the specification of a defined geometry for the post-treated plate edges, such as chamfer or a radius mentioned in the description.

In this context, the presented research aims to address those gaps by providing test results and recommendations that will offer extended guidelines and allow for a better evaluation of aforementioned details. In the past, numerous research projects have focused on the fatigue behavior of thermal cut edges. Most studies observe that cracks in the specimen typically initiate from the corners of the cut edges, e.g., Dieckhoff et al. [8], Lillemäe-Avi et al. [9], and Remes et al. [10]. Although some previous studies included post-treatment of the cut edge areas, these treatments were often vaguely described as deburring or grinding the edges. However, it is well known from the literature that, especially for notch-insensitive details like thermal cut edges, surface conditions and small defects significantly influence the performance in fatigue tests. Sperle [11] illustrates this behavior in the Kitagawa diagram shown in Fig. 3. The diagram shows that especially for the use of higher strength steels good surface properties are deemed required. Large defects or weak surface qualities do not lead to any significant increase in the fatigue properties of high-strength steels.

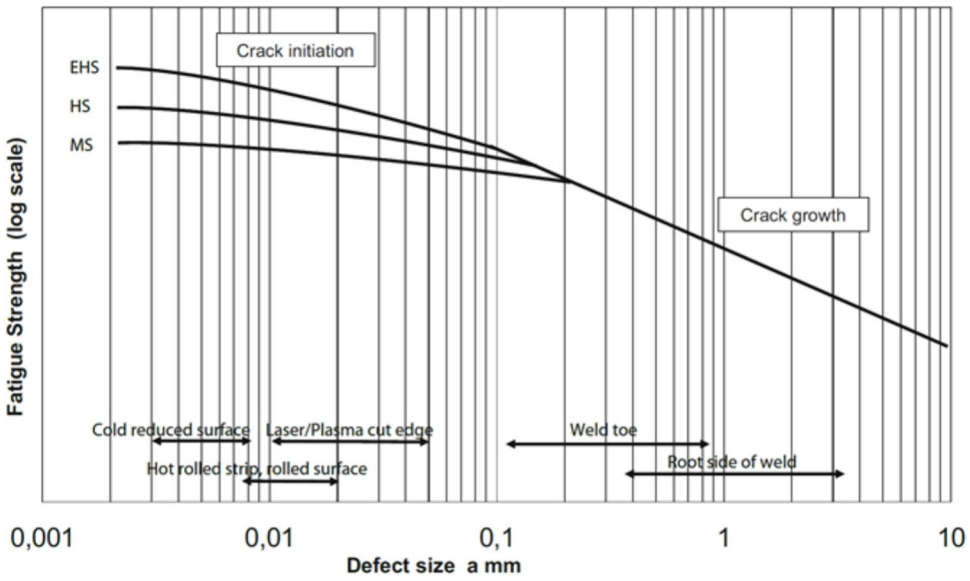

Fig. 3 Kitagawa diagram, schematic representation of defect size and achievable fatigue strength, illustrating the influence of material yield strength from normal-strength steels (MS) to high- and extra-high-strength steels (HS & EHS), especially for small defect sizes, adapted from [11]

The influence of cutting quality, e.g., characterized by the features recorded according to ISO 9013 [12], is well-documented through numerous studies but has not been sufficiently quantified and verified in the context of fatigue testing. The most clearly demonstrated influencing factor on the fatigue strength of thermal cut edges to state is the roughness depth R_z of the cut edge surface, e.g., Sperle [11], Stenberg et al. [13] and Diekhoff et al. [14]. However, these studies were mainly conducted on cut edges without any defined post-treatment. In these cases, crack initiation typically occurs at the sharp corner of the cut edge without post-treatment, as shown in Fig. 4. Only with very high cutting quality and simultaneous post-treatment of the critical notch an increase in fatigue strength could be detected when using higher strength materials, as presented by Diekhoff et al. [14]. In such cases, cracks initiate from the cut surface or ideally from the sheet metal surface. Studies like Lillemäe-Avi et al. [9], Remes et al. [10], von Bock and Polach et al. [15], and Kahl et al. [16] investigated steels with different yield levels, cutting technologies and edge treatments. In general, it could be seen that an increased material strength was beneficial regarding the achieved fatigue performance, but the results were not clearly in line to identify a summarizing material factor to describe the behavior sufficiently. The reason for the ambiguous correlation may lie in varying cutting quality and different types of post-processing.

These findings lead to the question how the effect of material strength and present surface qualities of thermal cut edges can be implemented in the fatigue lifetime assessment of structures. A promising path seems to follow the idea of a reduced notch effect of the cut edge corner by a certain treatment method and to define a requirement for the cutting process or surface quality to achieve repeatable production process standards. A sharp corner geometry causes high stress concentration and can be seen as potential location for crack initiation. The idea of a beneficial treatment regarding fatigue behavior is to smoothen this local detail by a more stress reducing shape like a radius or chamfer.

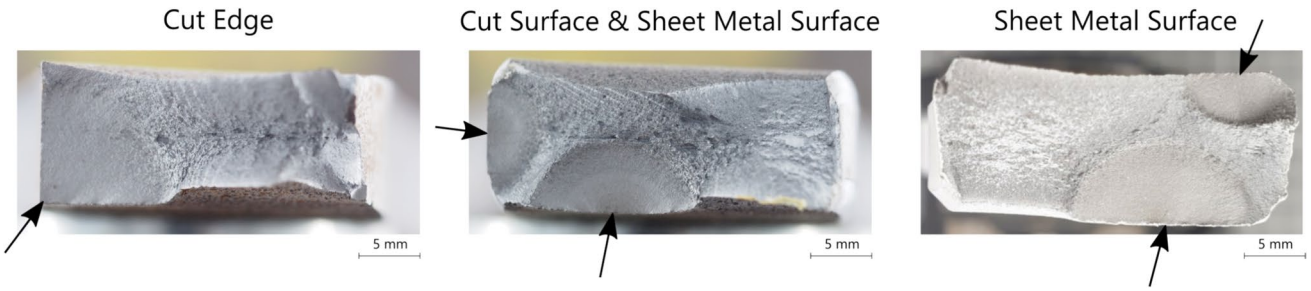

Fig. 4 Location for crack initiation during fatigue tests of thermal cut edges, location at corner of edge (left), cut surface (middle), and sheet metal surface (right), locations of crack initiation marked by arrows

2 Experimental investigations

The aim of this study is to investigate the fatigue behavior of cut edge details through experimental testing while evaluating the effect of a defined post-treatment method. For this purpose, specimen bodies are manufactured using different cutting technologies and subsequently analyzed for their properties. Different steel grades are considered to quantify the influence of the yield strength. The principal procedure is summarized in a flowchart shown in Fig. 5.

2.1 Specimen preparation

As described previously the aim of the study is to identify the effect of a defined edge treatment on the fatigue behavior of different material grades and cutting technologies. Therefore, specimens are designed to mirror the typical construction details of free plate edges and to have comparable notch effects. In shipbuilding constructions, various cutouts are provided with large radii to minimize local stress concentrations. In addition, the constraints of the testing machines were taken into account. As geometric boundary conditions, a length of 500 mm and a width of 80 mm in the clamping area of the specimens were established. The rounded shape of the cutouts was considered with a radius on both sides of the flat specimens, resulting in a specimen shape as depicted in Fig. 6. The specimen width in the tapered area was set to 30 mm. The radii were set to 500 mm, corresponding to the rounding of various openings in maritime structures. An overview of the specimen shape as well as the cut edge post-treatment by grinding of a chamfer is summarized in Fig. 6.

In order to investigate the effectiveness of the edge post-treatment as a measure to increase the fatigue properties of

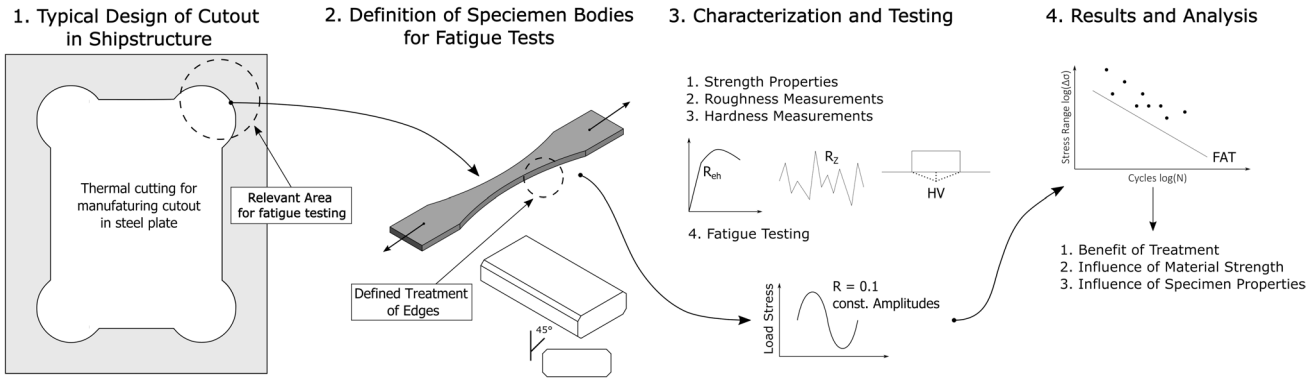

Fig. 5 Principal procedure of experimental investigations and following analysis of results

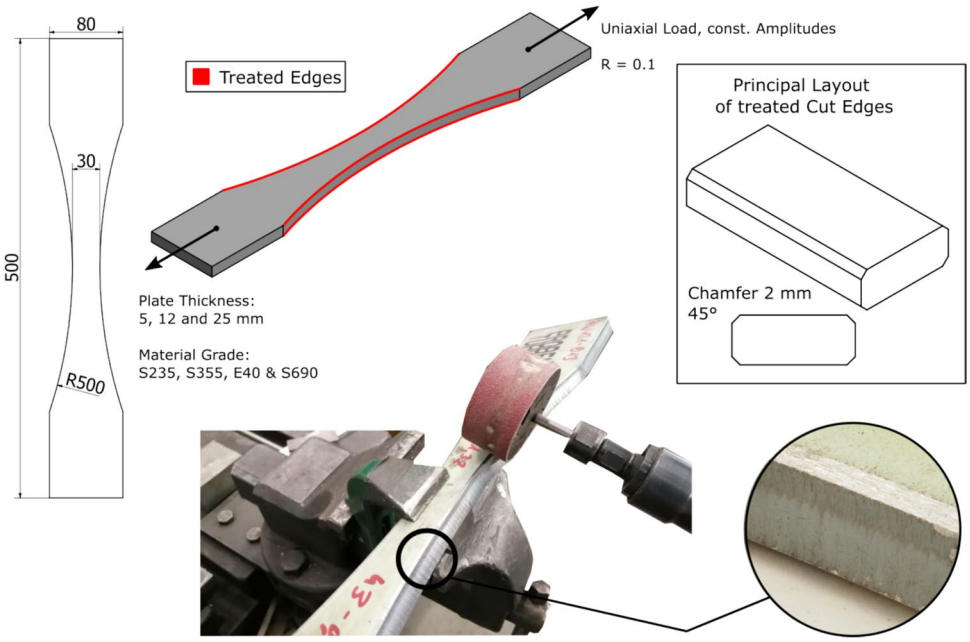

Fig. 6 Dimensions and layout of specimen bodies, illustration of applied loads and treatment method using grinder and round sanding sleeve

Table 1 Regarded steel grades, plate thicknesses, and cutting processes

	Material			
Cutting process	S235	S355	E40/S390	S690
Plasma	5 mm/12 mm	5 mm/12 mm	25 mm	12 mm
Plasma underwater	12 mm	12 mm	-	-
Flame cutting	12 mm	12 mm	-	-

thermal cut edges, samples of different steel grades in different plate thicknesses were prepared using different cutting processes and tested in accordance with Table 1.

2.2 Specimen and material characterization

Prior to the fatigue tests, the specimens underwent detailed characterization. This included tensile tests of the base material, angular distortion measurements, determination of surface roughness, and metallographic analysis of the cut edges. Following the tests, a fractographic analysis of the crack surfaces was conducted. The following sections describe the execution of the characterizations and the obtained results. The sampling positions for the different characterization methods are schematically depicted in Fig. 7.

2.2.1 Tensile properties of the base material

Due to the different steel materials from various suppliers considered in this study, the materials were subjected to a standardized tensile test to determine the mechanical properties according to DIN En ISO 6892–1. Figure 8 shows a comparison of the stress–strain curves obtained in the tensile test, exemplified by one representative curve for each material. The material properties determined, including R_{eH} (upper yield strength), R_{eL} (lower yield strength), R_m (tensile strength), and A_5 (elongation), are summarized in Table 2, depending on the cutting method used for producing the fatigue specimens. The results demonstrate that the material specifications are met in all cases. Notably, for the S355 grade specimens, it is evident that the material specifications are well exceeded, with the upper yield strengths ranging from $R_{eH} = 411$ to 555 MPa. In general, the materials exhibited significant differences between the upper and lower yield strengths. The differences in yield levels can be

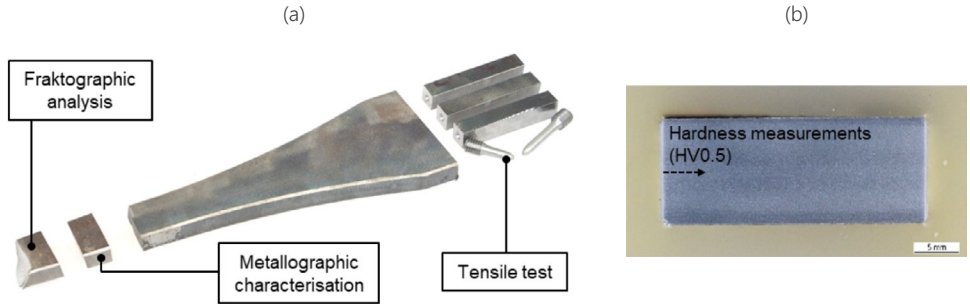

Fig. 7 Illustration of different characterization methods on specimen bodies (**a**) and path for hardness measurements within cross section of specimens (**b**). Round specimen bodies for tensile tests cut out of square end of large bodies to test base material properties

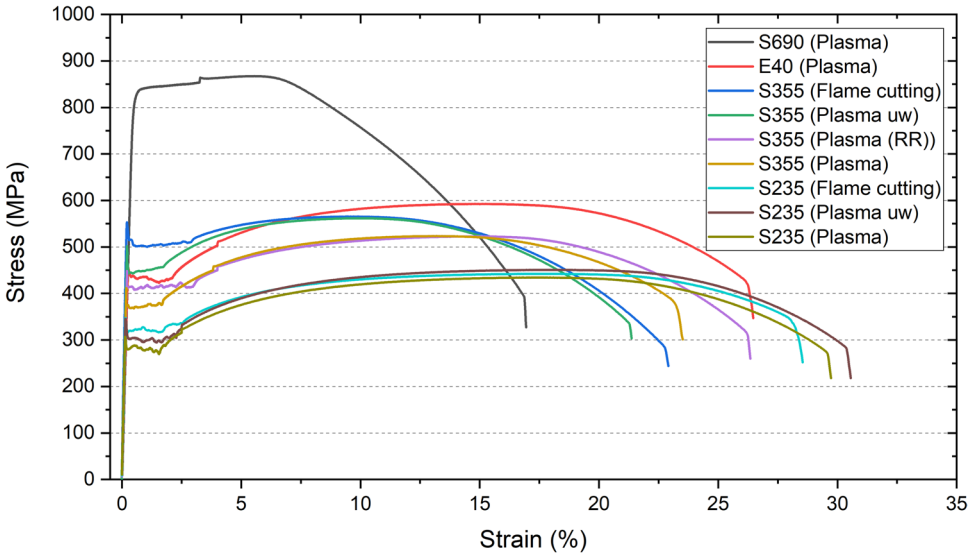

Fig. 8 Results of tensile tests for different specimen series (base material of each series)

Table 2 Summarized results of tensile test for all specimen series, results for base material of each series, listed according to cutting technique and material grade

Cutting process	Material	R_{eH} (MPa)	R_{eL} (MPa)	R_m (MPa)	A_5 (%)
Plasma	S235 (12 mm)	316.0 ± 14.9	274.9 ± 4.1	435.9 ± 3.8	29.8 ± 0.7
	S355 (12 mm)	410.9 ± 11.4	368.8 ± 3.9	528.0 ± 8.9	25.2 ± 2.3
	S355 (12 mm, RR)	441.5 ± 12.1	411.5 ± 4.8	524.9 ± 1.9	26.9 ± 4.7
	E40 (25 mm)	453.2 ± 4.9	428.1 ± 5.3	596.1 ± 5.6	26.7 ± 1.6
	S690 (12 mm)	860.7 ± 14.2	-	862.0 ± 13.8	17.1 ± 0.6
Plasma underwater	S235 (12 mm)	333.1 ± 19.1	293.6 ± 2.0	448.7 ± 1.7	27.5 ± 5.2
	S355 (12 mm)	505.9 ± 31.8	437.1 ± 15.4	557.7 ± 12.0	22.0 ± 2.2
Flame cutting	S235 (12 mm)	340.0 ± 12.9	314.1 ± 2.0	440.9 ± 1.0	29.0 ± 2.5
	S355 (12 mm)	555.0 ± 9.5	492.2 ± 6.6	558.6 ± 6.4	22.6 ± 1.0

attributed to the approach, that all specimen series were cut from different plate materials, provided by the manufacturing companies involved in this study.

2.2.2 Surface quality and roughness measurements

Surface roughness is a crucial criterion for evaluating the execution quality of thermal cutting processes and for the fatigue strength assessment. Accordingly, roughness was measured using a stylus instrument according to DIN En ISO 4288 in the relevant areas for the investigations: the cut surface, cut edge, and the original sheet metal surface. The measurements refer to the surfaces present after cutting and post-treatment of the cut edge. Figure 9 summarizes the average surface roughness R_z depending on the materials used, the cutting method, and the measurement locations. The average roughness measured on the sheet metal surface ranges from approximately 23 to 58 µm, consistently exceeding the roughness measured on the cut surface and cut edge. With few exceptions, the mean values of the average surface roughness measured on the cut surface fall within evaluation group 2 according to DIN En ISO 9013. Exceptions include the plasma cut samples of materials S690 and E40, which reach evaluation group 1. Samples produced by flame cutting exhibit significantly higher surface roughness. Consequently, the S355 series samples fall into evaluation group 3. The lower roughness depths measured for S235 can be attributed to a significant slag covering the cut surface. This could only be removed through mechanical treatment, which would have altered the surface condition. Therefore, measurements were performed in the as-manufactured condition. The roughness of the treated cut edges consistently shows comparable values with $R_z \leq 12$ µm.

2.2.3 Metallurgy and hardness measurements of edges

The metallographic investigations included both the microstructure formation in the heat affected zone (HAZ)

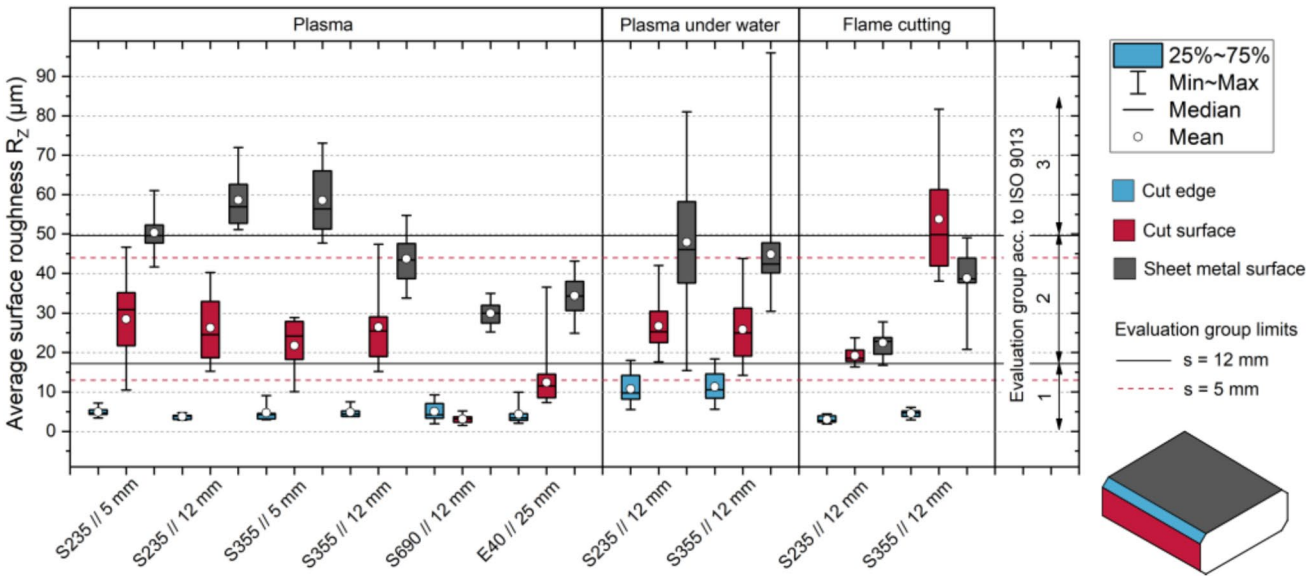

Fig. 9 Summarized results of roughness measurements for all test series; reference values according to ISO 9013

due to the cutting process and hardness measurements. The microstructure formation of the HAZ is shown in Fig. 10 using the example of the S355 plasma cut specimen with a 12-mm plate thickness. According to the heat input and cooling behavior, the edge area exhibits a predominantly martensitic microstructure. The martensitic microstructure gradually decrease with increasing distance from the cut surface. Since only unalloyed and low-alloyed steels were examined in this study, the microstructure formation of the HAZ mainly differs in terms of geometric width depending on the heat input and the cooling rate of the respective cutting processes.

The microstructure changes due to the thermal influence during the cutting process can be described by local changes in material hardness. This was characterized by microhardness measurements (HV0.5) along a measurement line perpendicular to the cut surface. Figure 11 shows the hardness measurements for the materials considered in this study, subdivided by the applied cutting process. Additionally, the width of the heat affected zone was determined based on the hardness profile. Generally, all materials and cutting processes show hardening near the cut surface with different maximum values and widths. For the structural steels S235 and S355 with 12 mm plate thickness, the use of plasma cutting (conventional and underwater) shows a comparable width of the HAZ. Regarding the maximum hardness, higher values are observed for the underwater cut samples due to higher cooling rates. The relatively high heat input combined with a slower cooling rate in flame cutting leads to a wider HAZ with lower maximum hardness. Samples with a smaller plate thickness (5 mm) show comparatively narrower hardening zones. Conversely, the width of the HAZ for E40 with higher plate thickness (25 mm) increases as expected. For the high-strength steel S690, an increase in hardness from approximately 300 HV0.5 to about 375 HV0.5 in the HAZ is observed. This is due to the martensitic components present in the base material and the associated high base material hardness.

2.3 Fatigue testing

The experimental investigations of the fatigue properties were performed using axial loading with a stress ratio of $R = 0.1$ until failure or until the limit of $N = 5 \cdot 10^6$ cycles was reached. After failure of a specimen, the fracture surfaces were examined regarding the location of crack initiation. The determination of the S–N curves with a 50% survival probability was performed according to the nominal stress approach. Additionally, the S–N curves for a survival probability of 97.7% were determined according to [3].

A servo-hydraulic universal testing machine (PLm630N, Walter + Bai AG) with a maximum dynamic load range of ± 400 kN and a test frequency of 8 Hz as well as a horizontally arranged resonance testing machine (Schenck) with a maximum load of 200 kN and a test frequency of approximately 33 Hz were used for the experiments. Both testing machines were aligned in this configuration before the tests and the setup was checked using a reference sample equipped with strain gauges.

The test results of all specimen series are shown in Fig. 12 and the characteristic values according to DVS [17] for each series are listed in Table 3. Within the diagrams, the S–N data points are further separated by the location of crack initiation of each specimen.

What stands out analyzing the test data is that all series show shallower slopes in a range of m = 5.5 to 23.4 compared to common guidelines by IIW [3] where a slope of m = 5 is proposed. In general, it can be stated that the data points, especially for series with steel grades of S355, E40, and S690, are well exceeding the highest reference design curve FAT140. Furthermore, it is clearly visible that an increase in material tensile strength directly affects the maximum stress ranges

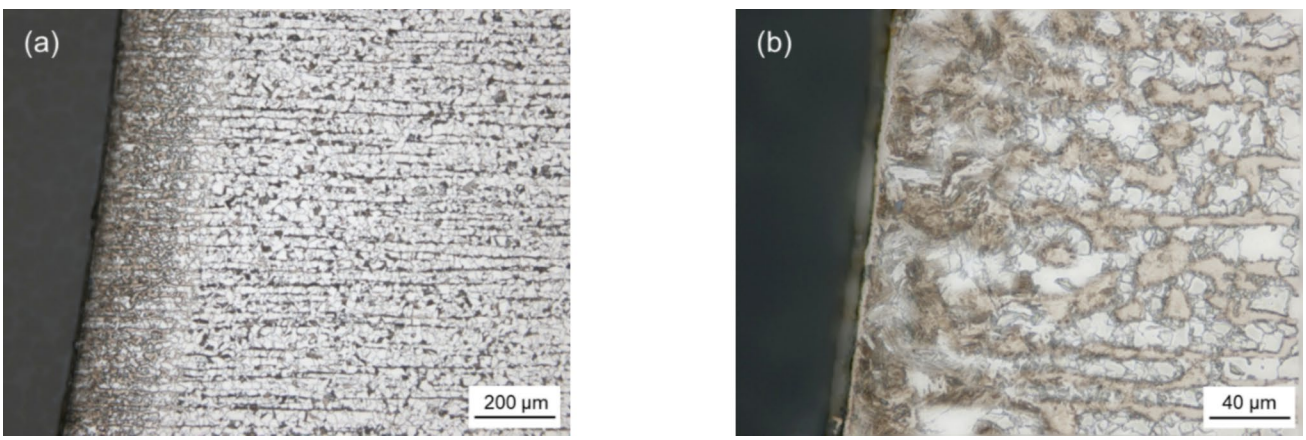

Fig. 10 Overview (**a**) of heat affected zone of cut edge (plasma cutting, 12 mm, S355) and detailed image (**b**)

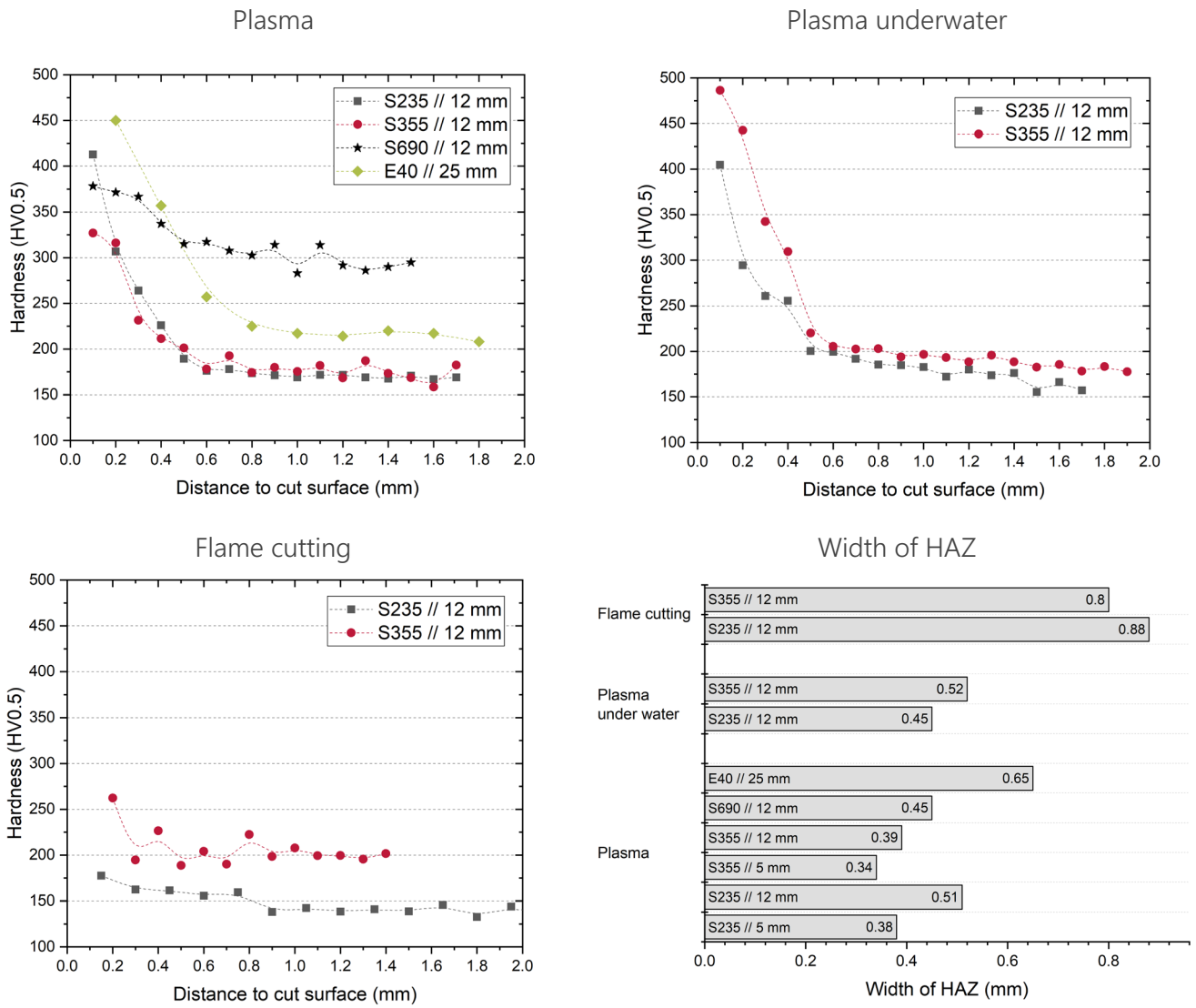

Fig. 11 Results of hardness measurements (HV0.5) and width of HAZ at cut edge; subdivided by cutting techniques

in fatigue testing, e.g., shown in S–N diagram for series cut by plasma underwater (Fig. 12) where specimens of S355 are clearly located above the data points of S235 specimen. A comparison of the three cutting technologies in this study does not reveal a clear influence of the method on the achieved fatigue strength. However, flame cutting seems to be more critical as the process tends to result in higher surface roughness at the cut edge as presented in Fig. 9. For the E40 series, it should be noted that five specimens were tested at stress levels slightly exceeding the yield strength according to the mentioned tensile tests. These load cases are highlighted in gray in the corresponding diagram. As the data points align well with the general scatter range, they were retained in the analysis.

Regarding the location of crack initiation, for most materials and cutting technologies, cracks predominantly originated from the cut surface or the sheet metal surface. Characteristic fracture surfaces are illustrated in Figs. 13 and 14. This leads to the conclusion that the sharp corner, which was the critical point for crack initiation in afore mentioned studies, could be attenuated by the chosen edge treatment and failures at this location were eliminated to large extend. Only in the series with high-strength material S690, it was noticeable that the crack initiation started at the plate surface next to the ground chamfer as shown in Fig. 14. Since these cracks were located adjacent to the edge, these data points are marked correspondingly. However, also the S690 series shows good agreement to the trend that increased material yield strength leads to a higher fatigue stress range. Therefore, the presented post-treatment can be considered as an effective way to utilize the potential of high-strength steels for thermal cut edges, with a focus on improving fatigue strength.

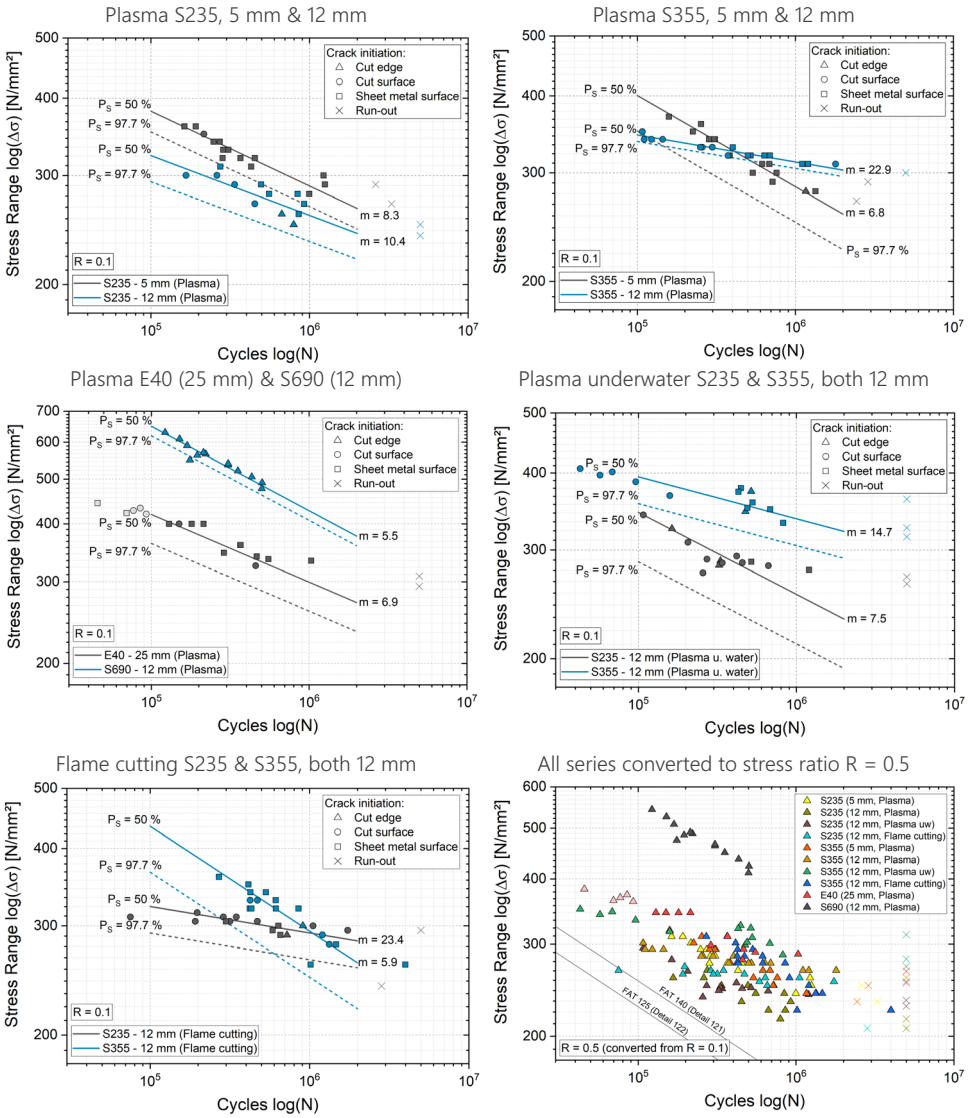

Fig. 12 S–N diagrams for all tested series, separated by cutting technology and material grade; summary of all test results (bottom right) converted to stress ratio of $R = 0.5$ compared to design curves FAT 125 and FAT 140 (m = 5) by IIW [3]

In addition to the achieved results listed in Table 3 all data points have been converted to a stress ratio of $R = 0.5$ for conservative and direct comparison to existing design curves by IIW [3]. The converted data is illustrated in Fig. 12. Using this conservative approach, it can still be noted that the fatigue results are located well above the stated design curves.

3 Influence of specimen properties on fatigue behavior

The previously presented experimental results demonstrate that the consistent post-treatment method of the cut edges can ensure comparable surface properties of the specimens cut edge. Due to these comparable properties among the different series, the influence of the respective material and its yield strength on the fatigue strength can be evaluated. The experiments revealed that an increase in the respective yield strength determined by tensile tests has a significant impact on the achieved fatigue strength. For instance, a comparison of the S235 and S355 material series with a 12-mm material thickness shows an increase in fatigue strength, which correlates well with the determined yield strength R_{eH}. Considering practical applications, in which strength design is typically based on the nominal yield strength, it was decided to classify the results presented here in the same manner. The use of yield strength instead of tensile strength also enables comparison with previous studies, e.g., [8, 9, 18], and DNV recommendations [1]. For a uniform comparison between the series, the mean values at a survival probability of 50% and a fixed slope of m = 5 were used. Table 3 provides reference values that may be used for comparison at a survival probability of 97.7%. The overview shown in Fig. 15 further indicates that the cutting technique seems to have a minor effect on the fatigue strength. Rather, the yield

Table 3 Results of fatigue tests summarized with calculated and fixed slopes ($\Delta\sigma$ calculated at $N = 2 \bullet 10^6$ cycles)

Cutting process	Steel	Thick [mm]	Slope m [-]	$\Delta\sigma_{50\%}$ [MPa]	$\Delta\sigma_{97.7\%}$ [MPa]	m = 3		m = 4		m = 5		m = 10	
						$\Delta\sigma_{50\%}$ [MPa]	$\Delta\sigma_{97.7\%}$ [MPa]	$\Delta\sigma_{50\%}$ [MPa]	$\Delta\sigma_{97.7\%}$ [MPa]	$\Delta\sigma_{50\%}$ [MPa]	$\Delta\sigma_{97.7\%}$ [MPa]	$\Delta\sigma_{50\%}$ [MPa]	$\Delta\sigma_{97.7\%}$ [MPa]
Plasma	S235	5	8.3	265	246	185	132	213	171	231	199	272	256
Plasma	S235	12	10.4	242	220	162	97	187	131	203	157	241	220
Plasma	S355	5	6.8	257	225	189	154	217	194	236	221	278	259
Plasma	S355	12	22.9	303	296	188	107	216	141	234	172	277	247
Plasma (round robin)	S355	12	17.9	346	331	197	122	234	166	259	199	317	286
Plasma	E40	25	6.9	271	234	180	126	216	166	241	208	299	273
Plasma	S690	12	5.5	377	359	275	235	326	299	362	343	446	413
Plasma underwater	S235	12	7.5	232	193	162	117	188	150	206	173	246	225
Plasma underwater	S355	12	14.7	322	291	186	103	221	145	245	179	301	267
Flame cutting	S235	12	23.4	284	257	185	110	209	142	225	167	261	221
Flame cutting	S355	12	5.9	262	221	237	147	254	177	264	203	285	243

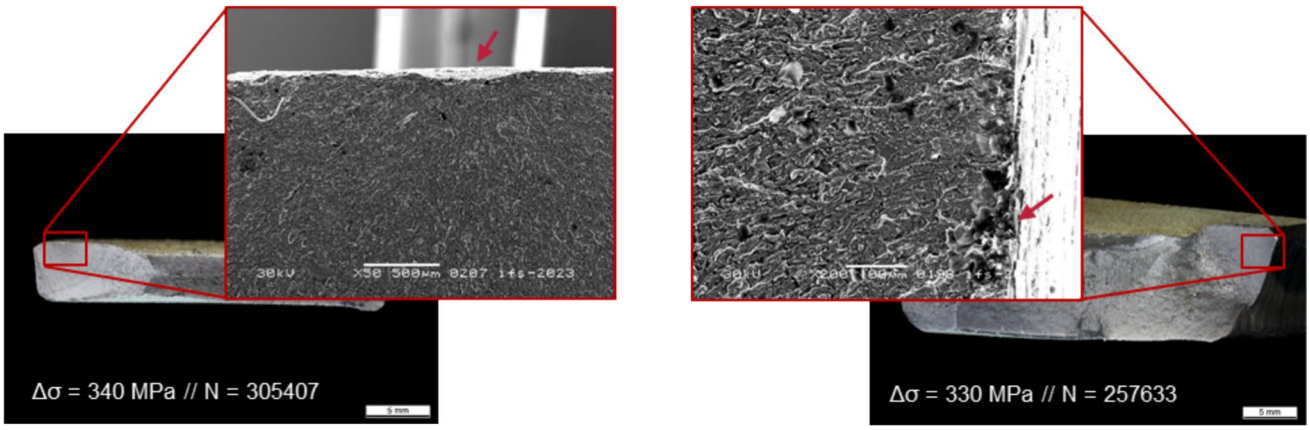

Fig. 13 Fracture surfaces of plasma cut S355 material in 5 mm (left) and 12 mml (right), crack initiation at sheet metal surface (left), and cut surface (right)

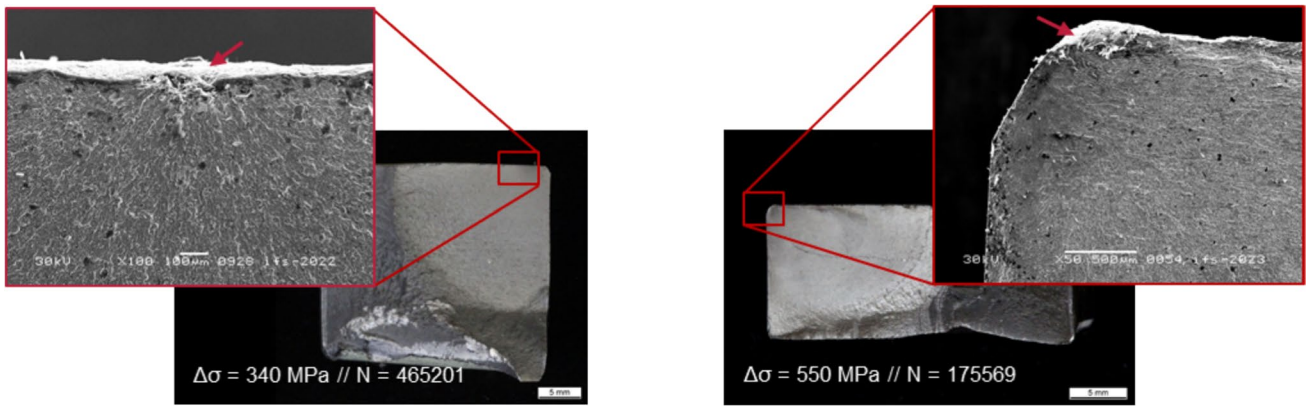

Fig. 14 Fracture surfaces of E40 specimen (left) and S690 material (right), crack initiation at sheet metal surface (left) and next to chamfer of edge treatment (right)

strength itself appears to be the key factor for the achieved results. It is important to note that, regardless of the cutting process, similar surface properties are present (Fig. 9), suggesting only minor differences in notch effects.

As expected, the specimen series with the lowest yield strength also represents the lower limit in fatigue strength, and the results in the S–N diagram in Fig. 15 consistently show an increase with rising strength. The curves exhibit a rise with increasing material strength, starting from $R_{eH}=316$ MPa up to 555 MPa. The differences are attributed to the fact that the sample series were produced by different suppliers, as described in Sect. 2.2.1, who used their own materials. Consequently, the series were not manufactured from a single batch. Looking at the results, only the underwater cut specimen series fall slightly below expectations compared to the other series. When examining the surface roughness values shown in Sect. 2.2.2, it is noticeable that the values at the chamfer in the corner area of the specimens, considered a critical notch for failure, are comparatively high at $R_z \sim 10$ µm for these two series. The other series exhibit a value of $R_z \sim 5$ µm in this area.

In the following, the possibilities for considering the strength of the respective steel in the assessment of fatigue behavior will be discussed. The material factor described in formula 1 and 2 according to DNV [1] provides an option to account for an increase in fatigue strength assessment through the use of higher strength materials. To evaluate this factor, the test results of the series were compiled with the fatigue strength parameter $\Delta\sigma_{97.7\%}$ at a number of cycles $N=2{\cdot}10^6$ over the respective yield strength in Fig. 16. The reference design S–N curve is FAT 140, which is corrected by the mentioned material factor depending on the yield strength according to the values given in Table 4. The individual test results are plotted for different specified slopes of m = 4, 5, and 10.

$$\triangle\sigma_{permissible} = \frac{FAT}{f_{material} \cdot f_i} \quad (1)$$

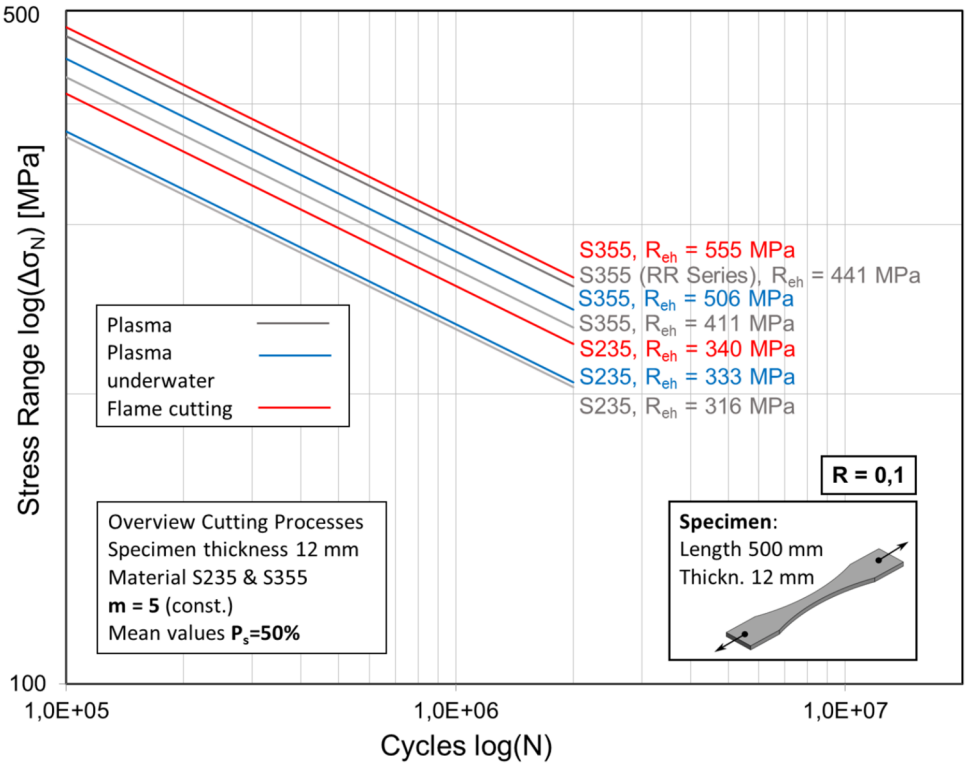

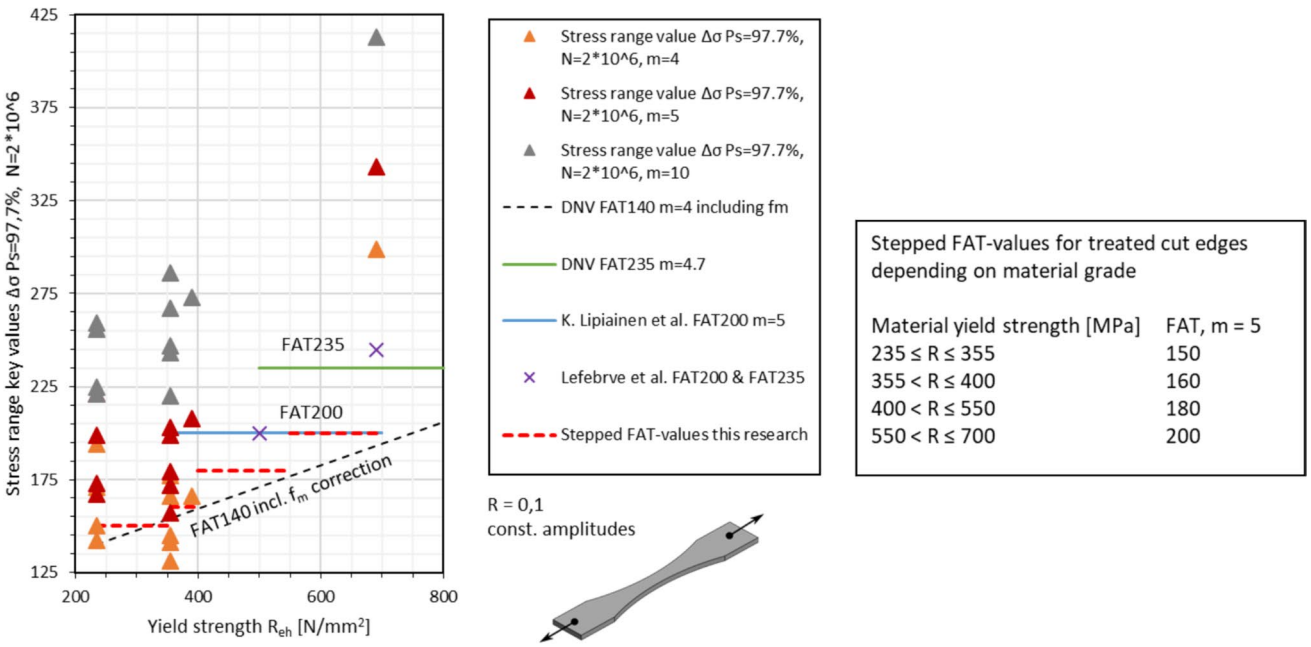

Fig. 15 Overview of test results of S235 and S355 material showing the influence of tested yield levels

Fig. 16 Resulting fatigue strength for different slopes (m = 4, 5, and 10) related to yield level according to steel grade; comparison to common design curves from recommendations and other research projects [18, 19]

Table 4 Overview of material factor by DNV affecting the reference FAT 140 depending on material grade

Steel grade and yield strength R_{eh} [N/mm^2]	Material factor $f_{material}$	Reference value FAT FAT 140/$f_{material}$
235	1	140
355	0.91	154
690	0.73	192

$$f_{material} = \frac{1200}{965 + R_{eh}} \quad (2)$$

f_i = further influencing factors for material thickness, mean stress, load spectra etc.

For higher strength materials, in particular, the question arises regarding an appropriate evaluation method with design S–N curves for the application of the nominal stress approach. Besides the mentioned material factor, DNV [1] offers the possibility, to apply the FAT 235 curve with a slope of m = 4.7 for steels with yield strengths above 500 MPa and the requirement of good surface qualities equal R_a = 3.2 µm or better. Findings by Lipiäinen et al. [18] dealing with the fatigue behavior of cut edges propose a FAT 200 curve with a corresponding slope of m = 5 for chamfered edges with yield strengths ranging from 350 to 700 MPa. Lefebvre et al. [19] proposed similar high values with FAT 163 for steel grades up to S400, FAT 200 for S500 material and FAT 245 for S690 steel. All mentioned S–N curves are shown as reference in Fig. 16.

Based on the series tested in this study, it is particularly evident that the respective slopes of the data points often run significantly shallower than indicated by existing design S–N curves. Therefore, it is considered reasonable to account for this behavior and propose using design S–N curves with a slope of m = 5 for post-treated cut edges. To incorporate the yield strength, it is suggested by the experimental results to design the applicable design S–N curve in steps depending on the material used. Similar approaches have already been implemented for the post-treatment of welded joints by IIW [20] and further investigated by other studies, e.g., Yıldırım et al. [21] and Braun et al. [22]. At the same time, it should be ensured that a safe and conservative design of the considered structure is maintained. Thus, it is proposed to divide the FAT characteristic values for post-treated cut edges into four steps for the investigated yield strengths ranging from 235 to 700 MPa. The arrangement is shown and listed in Fig. 16. For normal and higher strength steels up to 355 MPa, a curve of FAT 150 is proposed. For higher and high-strength materials, the curves FAT 160, FAT 180, and FAT 200 are presented as potential design S–N curves. This recommendation is in general more conservative than the previously mentioned and described curves by Lipiäinen et al. [18] and Lefebvre et al. [19]. However, it is important to note that within this study, only a few series with yield strengths above 355 MPa were tested, suggesting further investigations in the future to verify the proposal.

As previously indicated and described in the literature, in addition to the defined edge geometry, smaller defects, particularly due to surface roughness, have an influence on the fatigue behavior of cut edges. As outlined by Sperle [11], higher surface roughness negatively impacts the fatigue performance of cut edges. It is also noted that, for cut edges with roughness values of $R_z \geq 60$ µm, no significant gains can be achieved by using higher strength materials. A qualitative distinction of the groove direction is not further mentioned or described. Findings by Stenberg et al. [13] and Hultgren et al. [23] show similar relations between the roughness or yield strength and the fatigue behavior.

The specimens considered in this study, all have comparable geometry and surface properties. The metallurgical characterization showed no particular anomalies. However, it is evident that the two-specimen series cut using plasma underwater exhibit higher roughness on the ground chamfer (see Fig. 9) and fall below the expected values based on yield strength in comparison to the other series (see Fig. 12).

Figure 17 plots the fatigue strength at a survival probability of 50% (mean value) at the number of load cycles $N = 2 \cdot 10^6$ against the respective roughness at the chamfer and cut edge. The left diagram shows the results for roughness at the chamfer. It can be seen that while the roughness of the mentioned series lies noticeably above the average roughness values of the other specimens, the achieved fatigue strength does not significantly deviate from the other data points. The right diagram uses the roughness of the cut surface as the reference value. The series of S355 material cut using flame cutting stands out. However, this value, with high roughness, falls within the upper range of achieved fatigue strengths. Based on this analysis of various roughness values, no definitive statement can be made about a significant influence of surface roughness on fatigue behavior.

Therefore, the consideration was made to combine the surface roughness at the critical chamfer (corner area of the steel edge) and also at the cut edge with the material's yield strength into a factor, allowing a two-parameter analysis of the relationships affecting the achieved fatigue strengths. The aim of this factor is to enable a straightforward prediction of the fatigue behavior of cut edges as a function of their strength. The parameter F_{RS} is introduced to describe roughness and yield strength. Formula 3 and 4 describe this dimensionless factor. The evaluation showed good correlation of the test results, granting a gain through good surface qualities up to a roughness value of R_z = 12.5 µm at the ground chamfer and R_z = 33 µm at the cut edge. Thereby, higher roughness leads to a reduction in the factor.

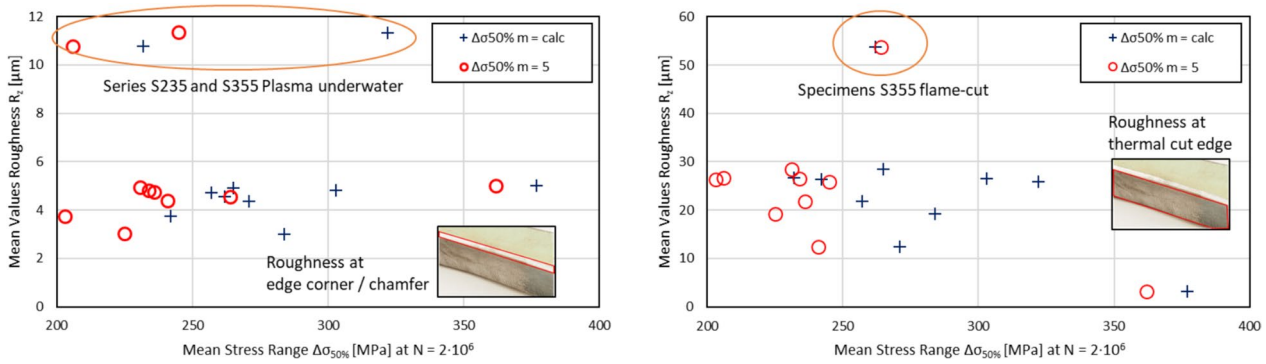

Fig. 17 Relation of measured roughness at edge corner/chamfer (left diagram) and at thermal cut edge (right diagram) to mean stress ranges of each series

$$F_{RS\ Chamfer} = \left(100 - 8 \cdot R_z\right) + R_e \quad (3)$$

$$F_{RS\ Cut\ Edge} = \left(100 - 3 \cdot R_z\right) + R_e \quad (4)$$

In Fig. 18, the F_{RS} factor is compared to the achieved fatigue strength for a survival probability of 50%. The left diagrams use the yield strength R_{eH} determined in the tensile tests and evaluates it with the fatigue strengths at a calculated and fixed slope of m = 5. It shows a good, nearly linear correlation of the factor with the mean fatigue strengths for the fixed slope, indicating that a higher F_{RS} values correlate with an increase in the respective fatigue strength for both roughness locations at chamfer and cut edge.

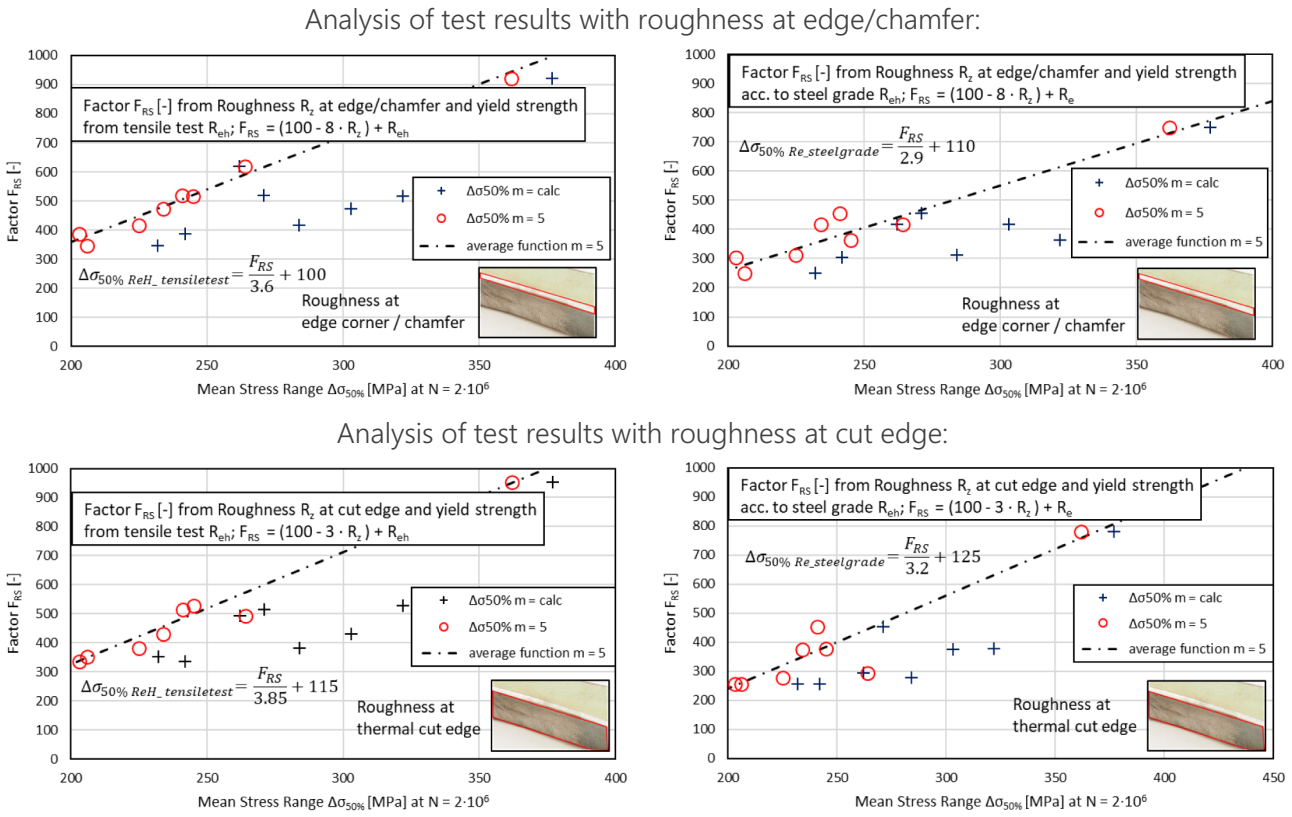

Fig. 18 Factor F_{RS} for roughness values at edge/chamfer (top) and at cut edge (bottom); values are calculated with the yield strength from tensile tests (left diagrams) and according to the minimal yield strength of each steel grade (right diagrams)

The right diagrams evaluate the factor using the minimum yield strengths according to the specifications of the steel grades from S235 to S690. This analysis also shows the previously observed trend for the fixed slope, although the scatter is higher compared to the reference values from the tensile test. Nonetheless, the mentioned factor appears to be a good indicator for capturing the relationship between material strength and the surface quality of post-treated cut edges. Hardness gradients and possible influences of residual stress were not further pursued since the evaluations described in Sect. 2.2.1 showed good correlation with the material's respective strength, deeming the inclusion of yield strength in creating the F_{RS} factor as sufficient. However, the described function can certainly be refined and possibly modified within the scope of further research.

To enable a prognosis of the achievable mean fatigue strength for a given strength and roughness, trend functions were created based on the evaluated results for a fixed slope of m = 5 in each diagram. These functions can thus illustrate the relationship between the F_{RS} factor and fatigue strength. The formulas in both left diagrams incorporate the yield strength R_{eH} determined from the tensile test, while formulas in right diagrams consider the nominal yield strength from the material specifications. All trend functions are plotted in the diagrams in Fig. 18.

These trend functions, like the previously described F_{RS} factor, can be seen as indications that need further verification for future applications. Particularly, the consideration of additional higher and high-strength steels should be pursued to improve the predictive capabilities for the fatigue strength of post-treated cut edges. The functions were created only for mean fatigue strengths at the number of load cycles $N = 2 \cdot 10^6$ and not for the usually applied survival probability of 97.7% in design S–N curves, as the scatter in the individual test series would render the functions less precise and not conducive to a meaningful conclusion. For the specimens tested in this study, the created factors and functions seem to accurately capture the fatigue behavior along with the properties. For conclusive predictions and especially for the transfer to design S–N curves, these approaches should be further investigated and evaluated based on an expanded data set.

4 Discussion

Within the study, ten series and one previous round-robin series of thermally cut specimens made from normal and high-strength steels, up to a yield strength of 690 MPa, were evaluated. Cutting methods used included flame cutting, conventional plasma cutting, and underwater plasma cutting. All specimen series were of good quality and were typically classified in Group 2 of 4 possible levels according to ISO 9013. Only one series of flame cut specimens exhibited larger grooves on the cut surface, resulting in a poorer rating of Level 3. Different companies, utilizing available plate material and cutting processes of their respective equipment, provided the specimen series. This approach allowed the consideration of different materials and, notably, the impact of individual yield strength on fatigue behavior, which was further examined in Sect. 2.

Previous test series described by Grimm et al. [24], considering edge treatment using CNC machines, achieved only slightly higher results in the fatigue behavior compared to the manual treatment method of a ground chamfer considered in this study. This suggests that the method used represents a viable option for effectively treating cut edges in order to increase the fatigue properties. It is assumed that other methods, showing comparable surface quality, could achieve similar fatigue strength results. The transferability should be examined case-by-case with respective users and further research. It is particularly important to specify that the processing must be performed along the length of the steel edge to avoid potential cracks from transverse grooves resulting from the grinding process.

The fatigue tests were conducted with a load ratio of $R = 0.1$, thus lying within the tension-tension range. The design S–N curves used in the standards are determined for a more conservative ratio of $R = 0.5$. Due to the relatively low notch effect in the practical test implementation, applying these conditions for the examined specimens is not feasible. The test results showed that even at $R = 0.1$, especially in series with very shallow slopes, only a narrow range of fatigue amplitudes covered the endurance limit range effectively in the test. Further increasing the load ratio and consequently the mean load in the test is not practicable. For translating the results into design S–N curves, there are recommendations for applying a reduction, such as those suggested by IIW [3]. This correction was done and presented in Fig. 12, which shows that achieved results are still above the FAT 140 design curve. However, this correction seems very conservative and for the sake of comparability to other studies in further calculations the initial stress ratio of $R = 0.1$ was kept.

Comparing the achieved results to the initially mentioned research gaps in Sect. 1.1, it can be summarized that the performed fatigue tests demonstrated that the yield strength of the material had the most significant impact on the achieved stress ranges. This influence was clearly illustrated in relation to previous studies, e.g., [18, 19], as the individual series exhibited comparable surface qualities and a consistent notch geometry due to the defined post-treatment. The question of the material's influence was answered, although additional tests with more series of different yield levels are deemed necessary for a final recommendation, given that only two series with higher strength steels beyond the commonly used S355 material in the maritime industry were considered. The tested materials E40 and S690 can be seen as good indicators for the properties of higher strength steels, which should be further verified. For the post-treated specimens considered in this study, it was notable that the slopes of the calculated S–N curves often flattened

significantly compared to the commonly cited values in the range of m = 3 to m = 5 in the guidelines like IIW [3], Eurocode 3 [4], and DNV [1]. This was also noted by other studies, e.g., von Bock und Polach [15]. The observed slopes were often considerably shallower, suggesting that these observations should be considered in future recommendations. The findings suggest that the slope exponent m = 5, as recommended by the IIW [3], appears to be the most appropriate. DNV [1] includes the consideration of material strength, which seems to be a suitable approach for thermal cut edges in general.

Although high-strength materials such as S690 still play a minor role in most shipbuilding applications, it is forward-looking to expand the current guidelines and regulations with corresponding FAT classes or correction factors to account for the potential of such materials.

For the recommendation of design S–N curves, it seems sensible to include the respective yield strength of the steel in the assessment, considering the required surface qualities and a defined post-treatment of the cut edge. The material factor described by DNV [1] accurately represents steels up to a yield strength of 355 MPa. However, steels with higher yield strengths, particularly high-strength materials with a yield strength of 690 MPa, are underestimated by this factor. This research indicates design S–N curves based on the tests conducted. The corresponding FAT values can be chosen in steps of FAT 150, FAT 160, FAT 180, and FAT 200 depending on the yield strength of the material used. A slope exponent of m = 5 is proposed for these curves. In formulating this type of recommendation, yield strength was preferred over tensile strength, as it is more practical to use, especially when design is carried out based on the nominal steel grade. These presented design curves are slightly more conservative than the stated recommendations from previous studies, e.g., Lipiäinen et al. [19]. However, these curves are above the proposed design curve for base material (FAT 160) proposed by IIW [3], that clearly shows the influence of the material strength plays in important role for the assessment of treated thermal cut edges and should be considered.

A proposed factor F_{RS} describes the relationships between the material strength and the respective surface qualities as trend functions, enabling a prognosis of the expected mean fatigue stress ranges at the load cycle $N = 2 \cdot 10^6$ for a fixed slope exponent m = 5. The factor should be investigated and validated with further data sets in the future.

5 Conclusions

The aim of this study was to investigate and determine the potential of a defined post-treatment and its influence on the fatigue behavior of thermal cut edges. Based on preliminary considerations, a chamfer was identified as an effective post-treatment for these details. The investigations showed that existing guidelines ensure a conservative assessment of the fatigue behavior of thermal cut edges. Regarding future applications of the findings, it was shown that thermal cut edges with good surface quality often exceed the highest design S–N curve FAT 140. Particularly, when using steels with yield strengths of 355 MPa and above, this FAT class can be used as a reliable basis if a good surface quality is given. Summarizing, this study aimed to address the question of improved assessment methods and a more targeted examination of these details, resulting in the following conclusions:

- The post-processing method used in this study, involving an air grinder and round sanding sleeve, showed high repeatability and positive effects on the fatigue behavior of the specimens. The tools used are common in metalworking companies, and the processes can be directly adopted by manufacturers. Special attention should be given to maintaining a consistent grinding direction along the length of the plate edge when applying the chamfer. In this study, the chamfer was made with a width of approximately 2 mm, applied to plates with thicknesses ranging from 5 to 25 mm.
- The fatigue tests demonstrated that nearly all specimens, regardless of their yield strength, are in general located above the higher design S–N curves of the recommendations (FAT 140). Thus, existing guidelines and regulations provide a conservative and safe assessment of the respective design details.
- The fatigue tests revealed that the resulting S–N curves tend to have much shallower slopes than the frequently cited slope m = 3 to 5 in the mentioned design guidelines and standards. This should be taken into account in future guidelines to better reflect the material behavior in the assessment. A slope exponent of m = 5, which is proposed in latest IIW recommendations [3], appears to be safely applicable and offer the possibility of a meaningful evaluation using the nominal stress approach with appropriate FAT values.
- This study indicates S–N curves based on the tests conducted on series including steel grades up to S690. The corresponding FAT values are proposed in steps of FAT 150, FAT 160, FAT 180, and FAT 200 depending on the yield strength of the material. The experimental results of this study demonstrate that the strength of the steel has a significant influence on the fatigue behavior of post-treated thermal cut edges A slope exponent of m = 5 is suggested for these curves.

Appendix

Table 5 Test results fatigue tests

S235, 5 mm, Plasma cutting					
Specimen No.	Stress-Ratio R [-]	Stress Amplitude [MPa]	Stress Range [MPa]	Cycles to failure N [-]	Comment
1	0,1	140	280	996970	
2	0,1	180	360	162815	
3	0,1	150	300	1225597	
4	0,1	160	320	283282	
5	0,1	155	310	429466	
6	0,1	135	270	3294506	Run-out
6*	0,1	170	340	248895	retested
7	0,1	145	290	2614060	Run-out
7*	0,1	165	330	307919	retested
8	0,1	175	350	216199	
9	0,1	165	330	286211	
10	0,1	145	290	1250649	
11	0,1	160	320	453250	
12	0,1	150	300	802928	
13	0,1	170	340	272425	
S235, 12 mm, Plasma cutting					
Specimen No.	Stress-Ratio R [-]	Stress Amplitude [MPa]	Stress Range [MPa]	Cycles to failure N [-]	Comment
1	0,1	135	270	452153	
2	0,1	150	300	260848	
3	0,1	140	280	842107	
4	0,1	140	280	555891	
5	0,1	145	290	337261	
6	0,1	155	310	273851	
7	0,1	135	270	924608	
8	0,1	145	290	495776	
9	0,1	130	260	669458	
10	0,1	120	240	10000000	Run-out
11	0,1	130	260	855119	
10*	0,1	145	290	243165	retested
12	0,1	125	250	795064	
13	0,1	150	300	166820	
S355, 5 mm, Plasma cutting					
Specimen No.	Stress-Ratio R [-]	Stress Amplitude [MPa]	Stress Range [MPa]	Cycles to failure N [-]	Comment
1	0,1	180	360	253183	
2	0,1	185	370	158347	
3	0,1	155	310	616523	
4	0,1	170	340	310128	
5	0,1	150	300	760571	
6	0,1	170	340	305407	
7	0,1	145	290	718003	
8	0,1	160	320	384201	
9	0,1	140	280	1340282	
10	0,1	160	320	501524	
11	0,1	135	270	2442255	Run-out
11*	0,1	175	350	224543	retested
12	0,1	150	300	537620	

Table 5 (continued)

13	0,1	145	290	2878438	Run-out
13*	0,1	170	340	284170	retested
14	0,1	155	310	684648	
15	0,1	140	280	1164241	
S355, 12 mm, Plasma cutting					
Specimen No.	Stress-Ratio R [-]	Stress Amplitude [MPa]	Stress Range [MPa]	Cycles to failure N [-]	Comment
1	0,1	150	300	4678977	Run-out
1*	0,1	165	330	298257	retested
2	0,1	165	330	257633	
3	0,1	160	320	499689	
4	0,1	160	320	690524	
5	0,1	170	340	144629	
6	0,1	175	350	107550	
7	0,1	155	310	1106629	s
8	0,1	170	340	110670	
9	0,1	165	330	402034	
10	0,1	160	320	637302	
11	0,1	155	310	1203997	
12	0,1	155	310	1796466	
13	0,1	170	340	122876	
14	0,1	165	330	250805	
15	0,1	150	300	5000000	Run-out
15*	0,1	160	320	521432	retested
16	0,1	160	320	375273	
E40, 25 mm, Plasma cutting					
Specimen No.	Stress-Ratio R [-]	Stress Amplitude [MPa]	Stress Range [MPa]	Cycles to failure N [-]	Comment
1	0,1	200	400	180285	
2	0,1	200	400	150002	
3	0,1	200	400	129572	
4	0,1	180	360	368389	
5	0,1	168	336	552200	
6	0,1	170	340	465201	
7	0,1	177	354	326355	
8	0,1	173	347	288515	
9	0,1	211	422	69775	
10	0,1	167	333	1030834	
11	0,1	147	293	5000000	Run-out
12	0,1	154	309	5000000	Run-out
13	0,1	162	325	458356	
14	0,1	199	399	122023	
15	0,1	222	444	45651	
11*	0,1	216	433	85060	retested
12*	0,1	214	428	77043	retested
S690, 12 mm, Plasma cutting					
Specimen No.	0,1	295	590	168667	
1	0,1	285	570	213985	
2	0,1	280	560	244719	
3	0,1	275	550	213691	
4	0,1	246	491	504133	
5	0,1	275	550	175569	
6	0,1	253	506	433314	

Table 5 (continued)

7	0,1	238	477	500733	
8	0,1	281	563	195459	
9	0,1	268	536	307026	
10	0,1	283	566	221059	
11	0,1	260	521	353649	
12	0,1	270	540	306778	
13					
14					
15					
S235, 12 mm, Plasma under water					
Specimen No.	Stress-Ratio R [-]	Stress Amplitude [MPa]	Stress Range [MPa]	Cycles to failure N [-]	Comment
1	0,1	171	342	107547	
2	0,1	162	325	163227	
3	0,1	154	309	205833	
4	0,1	147	293	419447	
5	0,1	139	279	1202231	
6	0,1	132	265	5000000	Run-out
7	0,1	136	272	5000000	Run-out
8	0,1	143	286	339986	
9	0,1	144	288	330440	
10	0,1	138	275	256588	
11	0,1	142	284	324337	
12	0,1	145	290	271685	
13	0,1	144	287	519080	
14	0,1	141	283	665447	
15	0,1	143	286	455953	
S355, 12 mm, Plasma under water					
Specimen No.	Stress-Ratio R [-]	Stress Amplitude [MPa]	Stress Range [MPa]	Cycles to failure N [-]	Comment
1	0,1	194	387	96286	
2	0,1	203	406	42919	
3	0,1	184	368	158361	
4	0,1	175	349	682877	
5	0,1	166	332	824809	
6	0,1	198	397	57275	
7	0,1	158	315	5000000	Run-out
8	0,1	179	358	527958	
9	0,1	187	374	517117	
10	0,1	163	326	5000000	Run-out
11	0,1	189	378	445878	
12	0,1	181	363	5000000	Run-out
13	0,1	173	347	475504	
14	0,1	186	373	430391	
15	0,1	176	351	489909	
8*	0,1	201	402	68459	retested
S235, 12 mm, Flame Cutting					
Specimen No.	Stress-Ratio R [-]	Stress Amplitude [MPa]	Stress Range [MPa]	Cycles to failure N [-]	Comment
1	0,1	120	240	2831592	Run-out
1*	0,1	150	300	638191	retested
2	0,1	155	310	288244	
3	0,1	145	290	656828	
4	0,1	153	305	299265	

Table 5 (continued)

5	0,1	150	300	1052300	
6	0,1	155	310	75178	
7	0,1	148	295	781992	
8	0,1	153	305	191953	
9	0,1	145	290	722664	
10	0,1	155	310	347510	
11	0,1	148	295	5000000	Run-out
11*	0,1	158	315	197185	retested
12	0,1	150	300	1673982	
13	0,1	153	305	316895	
14	0,1	148	295	1738591	
15	0,1	148	295	586484	
16	0,1	153	305	471013	
S355, 12 mm, Flame Cutting					
Specimen No.	Stress-Ratio R [-]	Stress Amplitude [MPa]	Stress Range [MPa]	Cycles to failure N [-]	Comment
1	0,1	160	320	852780	
2	0,1	170	340	532066	
3	0,1	165	330	471332	
4	0,1	150	300	909452	
5	0,1	160	320	615671	
6	0,1	140	280	1466675	
7	0,1	145	290	1205693	
8	0,1	160	320	421842	
9	0,1	140	280	1331088	
10	0,1	130	260	1015863	
11	0,1	180	360	270183	
12	0,1	130	260	3994676	
13	0,1	175	350	414177	
14	0,1	165	330	613730	
15	0,1	170	340	425941	
16	0,1	165	330	424335	
17	0,1	160	320	431975	

Author contribution Jan-Hendrik Grimm: writing—original draft—review and editing, visualization, methodology, testing, validation, formal analysis, investigation conceptualization, software; Markus Köhler: writing—original draft, visualization, testing, validation; Moritz Braun: validation, supervision, conceptualization; Franz von Bock und Polach: supervision; Klaus Dilger: supervision; Sören Ehlers: supervision.

Funding Open Access funding enabled and organized by Projekt DEAL. The work was performed within the research project Fatigue of Thermal Cut Edges in Shipbuilding Steel Structures, funded by the German Research Association of the Working Group of the Iron- and Metal-processing Industry e.V. as part of the Donors' Association for the Promotion of Sciences and Humanities in Germany under project number AVIF-No. A 322. The project was accompanied by a working group of Forschungsvereinigung Schiffbau und Meerestechnik e.V.—FSM (German Shipbuilding and Ocean Engineering Research Association) involved in the design of the study.

Data availability Relevant data given in appendix.

Declarations

Conflict of interest The authors declare no competing interests.

References

1. DNV, DNV-CG-0129 (2021) Fatigue assessment of ship structures, DNV. https://standards.dnv.com/explorer/. Accessed Dec 2024
2. DNV, DNV-RU-SHIP (2023) Pt.3 Ch.1: Part 3 Hull Chapter 1 General principles, DNV. https://standards.dnv.com/explorer/. Accessed Dec 2024
3. Hobbacher AF, Baumgartner J (2024) Recommendations for fatigue design of welded joints and components. Springer Nature Switzerland, Cham
4. EN 1993–1–9 (2005) Eurocode 3: design of steel structures — part 1–9: fatigue, Brussels
5. Fricke W, Paetzold H (2014) Effect of whipping stresses on the fatigue damage of ship structures. Weld World 58:261–268. https://doi.org/10.1007/s40194-014-0111-5
6. Li Z, Ringsberg JW (2012) Fatigue routing of container ships–assessment of contributions to fatigue damage from wave-induced torsion and horizontal and vertical bending. Ships Offshore Struct 7:119–131. https://doi.org/10.1080/17445302.2011.559368
7. Storhaug G, Moe E, Holtsmark G (2007) Measurements of wave induced hull girder vibrations of an ore carrier in different trades. J Offshore Mech Arct Eng 129:279–289. https://doi.org/10.1115/1.2746398
8. Diekhoff P, Hensel J, Nitschke-Pagel T, Dilger K (2019) Fatigue strength of thermal cut edges—influence of ISO 9013 quality groups. Weld World 63:349–363. https://doi.org/10.1007/s40194-018-00697-7
9. Lillemäe-Avi I, Liinalampi S, Lehtimäki E, Remes H, Lehto P, Romanoff J, Ehlers S, Niemelä A (2018) Fatigue strength of high-strength steel after shipyard production process of plasma cutting, grinding, and sandblasting. Weld World 62:1273–1284. https://doi.org/10.1007/s40194-018-0638-y
10. Remes H, Korhonen E, Lehto P, Romanoff J, Niemelä A, Hiltunen P, Kontkanen T (2013) Influence of surface integrity on the fatigue strength of high-strength steels. J Constr Steel Res 89:21–29. https://doi.org/10.1016/j.jcsr.2013.06.003
11. Sperle J-O (2008) Influence of parent metal strength on the fatigue strength of parent material with machined and thermally cut edges. Weld World 52:79–92. https://doi.org/10.1007/BF03266656
12. DIN EN ISO 9013:2017-05 (2017) Thermisches schneiden - einteilung thermischer schnitte - geometrische produktspezifikation und qualität; deutsche fassung EN_ DIN Media GmbH, Berlin
13. Stenberg T, Lindgren E, Barsoum Z, Barmicho I (2017) Fatigue assessment of cut edges in high strength steel – influence of surface quality. Materialwiss Werksttech 48:556–569. https://doi.org/10.1002/mawe.201600707
14. Diekhoff P, Hensel J, Nitschke-Pagel T, Dilger K (2020) Investigation on fatigue strength of cut edges produced by various cutting methods for high-strength steels. Weld World 64:545–561. https://doi.org/10.1007/s40194-020-00853-y
15. von Bock und Polach F, Kahl A, Braun M, Sperle J-O, von Selle H, Ehlers S (2023) Analysis of the scatter in fatigue life testing of thick thermal cut plate edges. Ships Offshore Struct 18:217–230. https://doi.org/10.1080/17445302.2022.2035562
16. Kahl A, von Bock und Polach F, von Selle H, Braun M, Grimm JH (2023, June) Yield strength and thickness effect on fatigue strength of thermal cut plate edges. In ISOPE International Ocean and Polar Engineering Conference (pp. ISOPE-I). ISOPE
17. DVS, Merkblatt DVS 2403, Empfehlungen für die Durchführung, Auswertung und Dokumentation von Schwingfestigkeitsversuchen an Schweißverbindungen metallischer Werkstoffe, DVS Media GmbH, 2019. https://www.dvs-regelwerk.de/regelwerke/merkblatt-dvs-2403-10-2020.
18. Lipiäinen K, Kaijalainen A, Ahola A, Björk T (2021) Fatigue strength assessment of cut edges considering material strength and cutting quality. Int J Fatigue 149:106263. https://doi.org/10.1016/j.ijfatigue.2021.106263
19. Lefebvre F, Lieurade HP, Huther I, Jubin L (2015) Proposal for fatigue classes applicable to thermal cutting, IIW document XIII-WG4–138-15. International Institute of Welding
20. Marquis GB, Barsoum Z (2016) IIW Recommendations on high frequency mechanical impact (HFMI) treatment for improving the fatigue strength of welded joints, IIW Recommendations for the HFMI Treatment 1–34. https://doi.org/10.1007/978-981-10-2504-4_1.
21. Yıldırım HC, Leitner M, Marquis GB, Stoschka M, Barsoum Z (2016) Application studies for fatigue strength improvement of welded structures by high-frequency mechanical impact (HFMI) treatment. Eng Struct 106:422–435. https://doi.org/10.1016/j.engstruct.2015.10.044
22. Braun M, Hensel J, Song S, Ehlers S (2021) Fatigue strength of normal and high strength steel joints improved by weld profiling. Eng Struct 246:113030. https://doi.org/10.1016/j.engstruct.2021.113030
23. Hultgren G, Mansour R, Barsoum Z, Olsson M (2021) Fatigue probability model for AWJ-cut steel including surface roughness and residual stress. J Constr Steel Res 179:106537. https://doi.org/10.1016/j.jcsr.2021.106537
24. Grimm J-H, Diniz e Castro J, von Selle H, Braun M, von Bock und Polach F, Ehlers S, Hensel J, Hesse AC, Dilger K (2022) The influence of edge treatment on fatigue behavior of thermal cut edges. In: ASME 2022 41st International conference on ocean, offshore and arctic engineering volume 2: structures, safety, and reliability. American Society of Mechanical Engineers (ASME), Hamburg, Germany. https://doi.org/10.1115/OMAE2022-7843